Millifluidics as a simple tool to optimize droplet networks: Case study on drop traffic in a bifurcated loop

William S. Wang and Siva A. Vanapalli

Citation: Biomicrofluidics **8**, 064111 (2014); doi: 10.1063/1.4902910
View online: http://dx.doi.org/10.1063/1.4902910
View Table of Contents: http://scitation.aip.org/content/aip/journal/bmf/8/6?ver=pdfcov
Published by the AIP Publishing

Millifluidics as a simple tool to optimize droplet networks: Case study on drop traffic in a bifurcated loop

William S. Wang and Siva A. Vanapalli[a)]
Department of Chemical Engineering, Texas Tech University, Lubbock, Texas 79409-3121, USA

(Received 12 September 2014; accepted 17 November 2014; published online 1 December 2014)

We report that modular millifluidic networks are simpler, more cost-effective alternatives to traditional microfluidic networks, and they can be rapidly generated and altered to optimize designs. Droplet traffic can also be studied more conveniently and inexpensively at the millimeter scale, as droplets are readily visible to the naked eye. Bifurcated loops, ladder networks, and parking networks were made using only Tygon® tubing and plastic T-junction fittings and visualized using an iPod® camera. As a case study, droplet traffic experiments through a millifluidic bifurcated loop were conducted, and the periodicity of drop spacing at the outlet was mapped over a wide range of inlet drop spacing. We observed periodic, intermittent, and aperiodic behaviors depending on the inlet drop spacing. The experimentally observed periodic behaviors were in good agreement with numerical simulations based on the simple network model. Our experiments further identified three main sources of intermittency between different periodic and/or aperiodic behaviors: (1) simultaneous entering and exiting events, (2) channel defects, and (3) equal or nearly equal hydrodynamic resistances in both sides of the bifurcated loop. In cases of simultaneous events and/or channel defects, the range of input spacings where intermittent behaviors are observed depends on the degree of inherent variation in input spacing. Finally, using a time scale analysis of syringe pump fluctuations and experiment observation times, we find that in most cases, more consistent results can be generated in experiments conducted at the millimeter scale than those conducted at the micrometer scale. Thus, millifluidic networks offer a simple means to probe collective interactions due to drop traffic and optimize network geometry to engineer passive devices for biological and material analysis. © *2014 AIP Publishing LLC*. [http://dx.doi.org/10.1063/1.4902910]

I. INTRODUCTION

Microfluidic drops are being used extensively as miniaturized reactors[1,2] for applications ranging from biological and material analysis[3–5] to material synthesis[6,7] to medical diagnostics.[8,9] Lab-on-chip platforms associated with these applications often involve the transport of nanoliter-scale droplets through networks of microchannels.[10,11] For example, past studies have designed microfluidic networks to passively coalesce, split, store, and sort drops.[12–20] Despite these demonstrations, it is still challenging, especially to design large-scale microfluidic networks that can manipulate droplets passively to achieve one or more functional tasks. The challenge lies in the fact that when confined droplets flow through networks even as simple as a bifurcation, they can exhibit complex spatiotemporal dynamics, depending on the branches they choose.[21–30] Since network architecture crucially impacts drop traffic, flexible methods are needed that can allow rapid generation of networks of varying architecture so that the optimal design can be constructed.

To aid in the design of microfluidic networks, models simulating drop traffic can be harnessed where droplets are treated as fluidic resistors and their traffic is modeled using simple

[a)]Author to whom correspondence should be addressed. Electronic mail: siva.vanapalli@ttu.edu.

pressure-flow rate relations.[31,32] Genetic algorithms have also been developed to search for optimal designs based on drop-traffic models.[33] Despite the ability of these models and simulations to yield networks that could perform a function or task, the designs have to be ultimately validated experimentally. However, experimental methods to efficiently create and modify network architecture have not been sufficiently developed. The availability of such methods will lead to coordinated modeling and experimental approaches for fast scanning and verification of optimal device designs.

To optimize device design using microfluidic networks requires microfabrication. In contrast, building millimeter-scale networks using commercial tubing and connectors is simpler and cost-effective, and it makes assembly and alteration of network architecture easier. Millifluidic networks can therefore serve as valuable scaled-up versions of microfluidic ones because the Reynolds numbers (Re) and capillary numbers (Ca) can also be maintained well below one, which are the key conditions in most microfluidic devices.[26,32] In fact, millifluidic devices are already being used for lab-on-chip applications.[34–36] Using commercially available transparent Teflon tubing, cross-junction connectors, and T-junction connectors, Trivedi *et al.* generated, stored, mixed, and optically detected aqueous droplets in oil.[34] They demonstrated the potential applications of modular millifluidics by creating a mix-and-read assay for dyed aqueous droplets and by culturing cells *in situ* within polymerized hydrogel droplets.[34] In another study, a millifluidic droplet analyzer was developed to find the minimum inhibitory concentration of antibiotic needed to kill bacteria.[35] A method to separate drops of different size based on collisions in a millifluidic network containing obstacles has also been demonstrated.[36]

In addition to these studies, modular millifluidic devices could be particularly useful in several different fields, such as chemistry, materials science, and biology. In chemistry applications, for example, millifluidic devices can be used to create micrometer- and millimeter-scale particles more easily and economically than with microfluidic devices while still benefiting from the high surface-area-to-volume ratios that improve heat transfer between phases.[37] Millifluidic devices could also be used to create new fluid-based materials such as multiple emulsions and Janus particles.[37,38] Since many biological assays involve handling of millimeter-scale objects, such as tumor spheroids, small animals, embryos, etc. (which are too large for microfluidic channels), drop-based millifluidics also has the potential to become an active area in biology.

Despite the significance of millifluidic devices for bioanalytical applications, only a few studies[21,29] have investigated drop traffic through modular millifluidic branching networks, even though important differences exist between millifluidic and microfluidic networks in terms of channel geometry. First, the conduit cross-section in millifluidic devices is typically circular, whereas in planar microfluidic devices it is rectangular or square. In addition, unlike in typical microfluidic devices, abrupt changes in cross-section are inherently present due to the use of fittings and connectors. The importance of these two geometrical factors in influencing the flow resistance of droplets and thereby traffic in networks needs to be investigated before the millifluidic approach can be readily used for designing and optimizing large-scale droplet networks.

The goal of this study is two-fold. We first demonstrate that modular millifluidic networks can be easily and rapidly constructed to study drop traffic in branching networks. Second, we study in detail the most elementary network possible—a millifluidic loop. We quantify the traffic behavior in this network and compare it with model predictions. We show the ease with which droplet behaviors can be characterized and compared with models of drop traffic. We also draw useful insights into the physics of drop traffic in a loop and illustrate how geometrical defects can influence traffic. Finally, we conclude with some remarks on the benefits of using millifluidic networks for studying drop traffic.

II. RESULTS

A. Quick assembly of millifluidic bifurcated loop network

To create simple millimeter-scale networks, the only materials needed are commercially available, transparent (or translucent), small-diameter tubing and connectors, such as T-junctions

and cross junctions (see Sec. IV). In addition to the ease of device assembly, a second advantage is the ability to see droplet production and movement with the naked eye. This means that research-grade laboratory microscopes are not necessary, and consumer cameras (e.g., iPod®) can be used to capture and study droplet motion. A third advantage is the ease with which such millifluidic devices can be modified. Network segments can be modified simply by detaching the tubing from the connectors and replacing them with different tubing and/or connectors. In contrast, traditional microfluidic devices cannot be altered after fabrication. Alternative network designs could therefore be manufactured more quickly and more easily on a millimeter scale than on a micrometer scale.

We demonstrate the usefulness of millifluidic networks by building and testing a millimeter-scale bifurcated loop (Fig. 1), which is created by simply joining lengths of commercially available Tygon® tubing and plastic T-fittings. When a train of uniformly spaced droplets enters the loop, diverse behaviors are possible at the exit of such a loop. Drops can exit the loop at periodic or aperiodic time intervals depending on the spacing with which drops enter the loop (see Movies S1, S2, and S3 in the supplementary material).[39] In Sec. II B, we illustrate how such a simply made network can be used to confront model predictions and reveal important insights into the causes for the transitions between periodic and aperiodic regimes.

B. Case study: Characterization of drop traffic in a millifluidic loop

The bifurcated loop is one of the simplest branching networks, having only two branches between a single inlet and a single outlet. While droplet traffic has been studied to some extent in more complex geometries,[40] fascinating and diverse behaviors are still possible from such a simple geometry as a bifurcated loop. Several studies of microfluidic loops have already been conducted and have revealed a wide variety of phenomena including: periodic and aperiodic behaviors,[26] reversibility of droplet train transformation,[26,31] coding and decoding of signals,[26] chaos,[41] multistability,[27] Hamiltonian dynamics,[42] filtering and repartitioning of droplet trains,[28,43] path selection,[44,45] and measurement of droplet resistance.[46]

While studies have explored droplet traffic through bifurcated loop networks[25–27,30,47] and developed models,[27,28,31,41,48] there are still unanswered questions. For example, what is the cause of transitions between periodic and aperiodic behaviors, and what affects those transitions? How do structural defects in the channels affect droplet traffic? To address these questions requires an experimental strategy where drop traffic behavior can be explored over a wide range of input droplet spacings without the complications of drop break-up and coalescence. Here, we show how a millifluidic loop network and an iPod® camera can be used to (1) rapidly scan drop traffic and identify flow conditions that are devoid of drop breakup and coalescence,

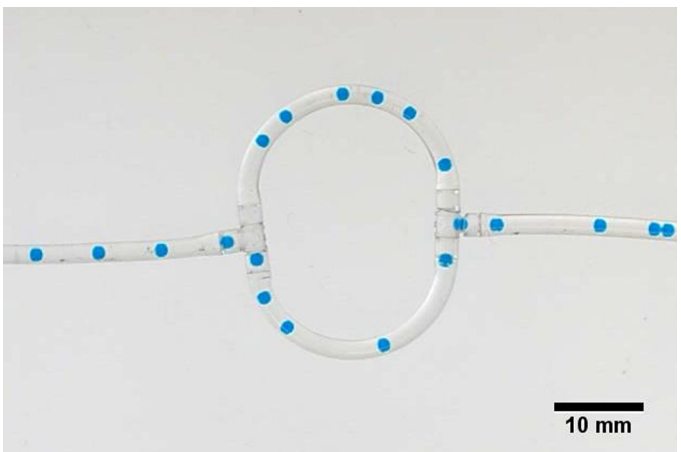

FIG. 1. A millifluidic bifurcated loop assembled using commercial T fittings and Tygon® tubing (1.25 mm inner diameter). Loop is a slightly asymmetric bifurcated loop, with a 44 mm-long upper branch and a 39 mm-long lower branch.

(2) characterize drop spacing at the exit in terms of two quantitative methods: Poincare maps and the droplet spacing quantization rule, (3) test experimental data with traffic model predictions, and (4) gain insights into the sources of intermittent and aperiodic drop dynamics at the loop exit.

1. Rapid scanning of drop behavior in a millifluidic loop

The millifluidic loop chosen for droplet traffic experiments is a slightly asymmetric bifurcated loop as shown in Fig. 1, with upper and lower branch lengths (L_u, L_l) of 44 mm and 39 mm and a branch-length ratio of $L_u/L_l = 1.12$. The drop size was manipulated by using a T-junction drop generator, and drop spacing was adjusted using an auxiliary channel downstream of the T-junction but upstream of the loop. To identify the potential operating conditions for studying drop traffic in the loop, the oil flow rate delivered to the droplet-producing T-junction was kept constant at $Q_o = 10$ ml/h, while the water flow rate Q_w and auxiliary oil flow rate Q_a were allowed to vary.

Fig. 2 is a behavioral diagram on a plot of flow rate ratio (Q_w/Q_o) versus total continuous phase (oil) flow rate ($Q_c = Q_o + Q_a$) showing four major droplet behaviors. We find that as the flow rate ratio (Q_w/Q_o) increases, droplet size increases. Also, as total oil flow rate (Q_c) increases, both droplet velocity and droplet spacing (λ) increase. As shown in Fig. 2(c), shear-induced splitting is observed at higher velocities for small droplets and at lower velocities for larger droplets. Droplet coalescence occurs when droplets are not so large that they undergo shear-induced break-up but are still large and close enough to have a high probability of colliding into each other at the loop exit (Fig. 2(d)). Behaviors well suited for studying droplet traffic (labeled "ideal") occur in the lower section of the diagram where droplet sizes are smaller, as smaller droplets are less likely to be fragmented. No hydrodynamic feedback ("no-H.F." or "no-feedback") between neighboring droplets, where each droplet's behavior at the loop entrance is not affected by the behavior of the surrounding droplets, occurs for small flow-rate ratios (small droplets) and large λ, as each droplet exits the loop before the next one enters.

Therefore, the best operating conditions for studying droplet traffic are when (1) droplets are relatively small but still confined or nearly confined so that they still impart significant hydrodynamic resistance, (2) there is no coalescence at the exit, and (3) when λ is less than the maximum $\lambda(\lambda_{max})$ for which there is still hydrodynamic feedback between neighboring droplets.

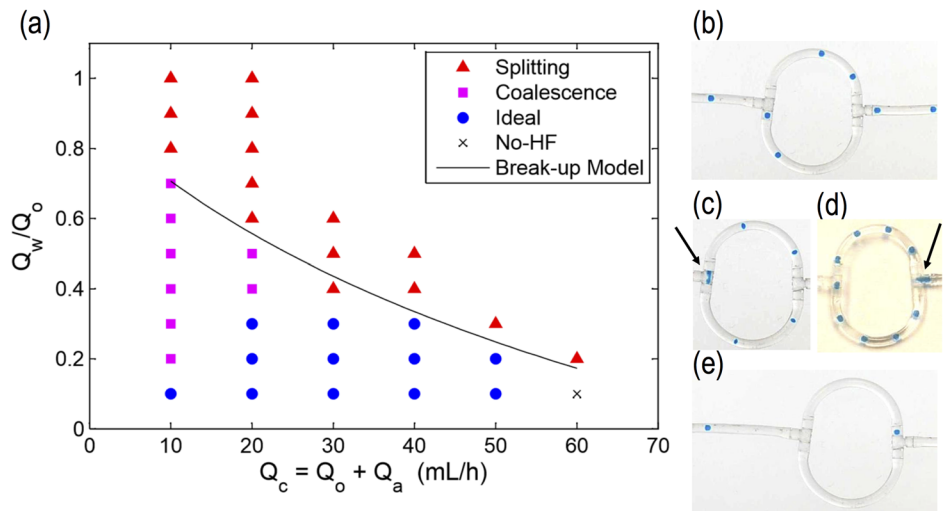

FIG. 2. Behavioral diagram for aqueous droplet trains in mineral oil passing through a slightly asymmetric millifluidic loop as shown in Figure 1. Ideal (b), splitting (c), coalescence (d), and no-hydrodynamic-feedback (e) behaviors are shown on a plot of flow rate ratio versus total continuous phase flow rate. Example experimental images are also included for those behaviors. Arrows in (c) and (d) indicate where drop break-up and coalescence are occurring, respectively. Fluid flow is left to right.

Thus, flow rate ratios ranging from 0.1 to 0.2 and total oil flow rates of less than 60 ml/h are the best operating conditions for probing droplet traffic.

We also sought to predict the drop break-up conditions observed in our experiments, as it will be a useful means to quickly assess the operating space for drop traffic. Several works have studied the conditions for droplet breakup in various conditions, such as at junctions of arbitrary angles[18] and upon impingement against an obstacle[19,20] within a confining channel. Link *et al.*[49] proposed a relation (Eq. (1)) for drop breakup at a microfluidic T-junction consisting of rectilinear channels, and we assessed whether this relation could also quantify drop breakup observed in our circular cross-sectioned channels. In Eq. (1), Ca* is the critical capillary number for droplet breakup, α_L is fitting parameter of Link *et al.*, and ε is the non-dimensionalized drop size as prescribed by Eq. (2), where l and w are the length and width of the drop, respectively,

$$Ca^* = \alpha_L \varepsilon (\varepsilon^{-2/3} - 1)^2, \tag{1}$$

$$\varepsilon = \frac{1}{\pi}\left(\frac{l}{w}\right). \tag{2}$$

Because our data in Fig. 2 are represented in terms of flow rates, we translated drop size to flow rate ratio (Q_w/Q_o) using Eq. (3), which was developed by Garstecki *et al.*[50] for droplets produced at a microfluidic T-junction. In Eq. (3), α_G is a fitting parameter

$$\frac{l}{w} = 1 + \alpha_G \left(\frac{Q_w}{Q_o}\right). \tag{3}$$

Combining Eqs. (1)–(3), we get Ca^* as a function of flow rate ratio and the two fitting parameters

$$Ca^* = \frac{\alpha_L}{\pi}\left(1 + \alpha_G \frac{Q_w}{Q_o}\right)\left(\left(\frac{1}{\pi} + \frac{\alpha_G}{\pi}\frac{Q_w}{Q_o}\right)^{-2/3} - 1\right)^2. \tag{4}$$

As shown in Fig. 2, we found good agreement between our breakup model (Eq. (4)) and experimental results when $\alpha_G = 1.4$ and $\alpha_L = 0.027$. We note that the value of α_G obtained in our millifluidic experiments is similar in magnitude to that in the microfluidic study. However, α_L in our experiments was two orders of magnitude smaller than that reported in the microfluidic study of Link *et al.* This is most likely because in experiments of Link *et al.*, the droplets were in square cross-sectioned channels,[49] which allows significant oil flow through the channel corners (gutters). In contrast, our millifluidic tubing has a circular cross-section, and therefore less space for oil to pass between the droplets and the channel walls. The shear stresses acting on droplets at a bifurcation should be much greater in the circular-cross-sectioned case than in the square-cross-sectioned case, and the critical capillary number should occur at much lower flow rate ratios. In Sec. II C 1, we provide a scaling analysis for the shear stresses in circular and square conduits that yield a reasonable estimate of the α_L value observed in our experiments. Thus, Eq. (4) is a useful guide for rapidly identifying conditions for studying drop traffic.

Interestingly, it took only 2–3 h to assemble the loop network and to perform all 36 experiments for the behavioral diagram, as each flow-rate setting appeared to stabilize within a matter of seconds. In contrast, pump fluctuations tend to occur on a much longer time scale in microfluidic experiments than millifluidic ones because syringe pumps generally must be operated at slower rates (see Sec. II C 4 for additional discussion). Thus, for each new millifluidic network, the best operating conditions could be determined within few hours, which is a significant advantage over microfluidic networks.

2. Characterizing the exit droplet spacing

Having identified the flow conditions at which drop traffic can be investigated, we characterized the drop spacings at the exit of the loop. Previous studies of microfluidic bifurcated

loops have shown that the exit drop spacings can follow either periodic or aperiodic behaviors.[26–28] Note that when we use the term "aperiodic" to describe output spacings in experiments, we mean only that there was no apparent repetition of any sequence within the observed finite train of droplets.

A common way to characterize the periodic or aperiodic nature of the transformed droplet spacing is to use Poincare maps.[26] A more recently proposed method is the droplet spacing quantization rule. Below, we apply both methods to our experimental data and also contrast the appropriateness of each method.[24]

a. Poincare maps. Poincare maps are graphical representations of the diversity in neighboring relationships, and they are created by plotting each time interval between droplets (Δt_{n+1}) versus the previous time interval (Δt_n). Because our systems have constant volumetric flow rates and constant cross-sectional flow area, comparing exit time gaps between droplets is the same as comparing exit spacings. Figure 3 includes exit Poincare maps for four example experiments conducted at different inlet spacings, with exit spacings (and exit time gaps) exhibiting period-2, period-4, aperiodic, and intermittent behaviors. In each experiment, roughly 150 or more evenly spaced droplets were sent through the bifurcated loop.

In the period-2 behavior shown in Fig. 3(a), the repeating pattern of exit time intervals (in seconds) is 3 5 3 5 3 5… Since the repeating pattern is [3 5], the Poincare map would have two points: (3,5) and (5,3) consistent with the two clusters shown in Fig. 3(a). Note how in the periodic cases (Figs. 3(a) and 3(b)) and in the intermittent case (Fig. 3(d)), the repeating exit patterns collapse into just a few clusters in the Poincare maps, whereas in the aperiodic case (Fig. 3(c)), the points in the map appear to be distributed randomly. In Figure 3(d), the exit patterns were primarily period-4 behavior (outer four clusters), but period-3 (inner three clusters) occasionally appeared. We use the terms "primary" and "secondary" to describe the dominant and subordinate intermittent periodic behaviors in those cases where one behavior clearly occurs more often than the other. For example, in Fig. 3(d), period-4 behavior occurred 31 times and period-3 behavior occurred 15 times in a train of 169 droplets. In some cases, several different behaviors occur without any one behavior dominating, in which case all of the observed periodic behaviors are secondary periodic behaviors (i.e., no primary periodic behavior).

In Fig. 3, we also included exit event-time plots[23,26] beneath each Poincare map as another means for visually depicting any underlying periodic behavior. Brackets have been included over some of the repeating units of events, and two different levels of brackets are shown in Fig. 3(d) for the intermittent period-3 and period-4 behaviors. As can be seen in Fig. 3(a), there is a pattern of time gaps that repeats every two events, thus the period length is two droplets long (period 2). The pattern in Fig. 3(b) repeats every four events, so the period length there is 4 droplets long (period 4). There is no discernible pattern in the aperiodic example in Fig. 3(c). In Fig. 3(d), the events occur in patterns of three or four events (intermittently period 3 or period 4), although it could also be viewed as patterns of four or seven events (intermittently period 4 or period 7).

b. Droplet spacing quantization. An alternative method for characterizing periodic pattern length (i.e., periodicity) is the droplet spacing quantization rule reported by Maddala *et al.*[24] Based on a principle of conservation of volume, Maddala *et al.* found that between any given point in one pattern and the same point in the next pattern, the volume of fluid between those two points is always the same no matter which point in the repeating pattern is chosen. More importantly, that volume of fluid is always an integer multiple of the volume of fluid between two droplets in the inlet channel (see Fig. 4). Because the cross-sectional area is constant throughout the system, this means that the total distance between sister points in two consecutive patterns is always an exact multiple of the inlet spacing. The droplet spacing quantization rule[24] in mathematical terms is given by

$$\sum_{j=n}^{n+P} \lambda_j = P\lambda_i, \tag{5}$$

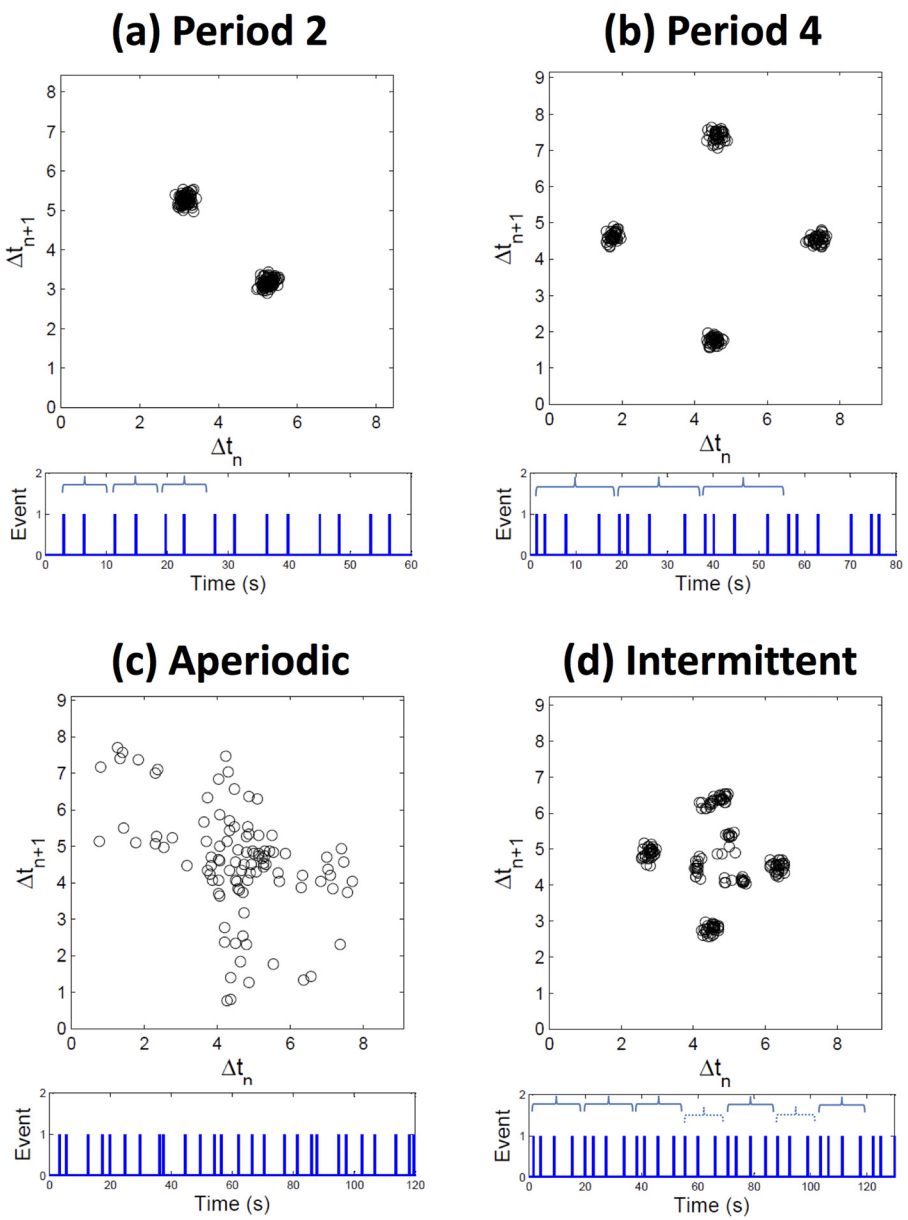

FIG. 3. Example Poincare maps for time gaps (in seconds) between exiting droplets showing (a) period-2, (b) period-4, (c) aperiodic, and (d) intermittent behaviors—with both period-3 and period-4 in (d). The initial spacings (λ) for the experiments were 56, 24, 12, and 32 mm for (a)–(d), respectively. Beneath each Poincare map is an event-time plot for droplet exit events, with repeating patterns bracketed. Two levels of brackets are shown in (d) for period-4 and period-3 behaviors.

where P is periodicity, n is any exit droplet identification number, λ_j is the j^{th} droplet exit spacing, and λ_i is the inlet spacing.

Applying Eq. (5) to the scenario shown in Fig. 4 implies that $\lambda_1 + \lambda_2 + \lambda_3 + \lambda_4 = 4\lambda_i$, i.e., the sum of four consecutive exit spacings exactly equals four times the inlet spacing—therefore, periodicity P = 4. Larger multiples of four (e.g., 8, 12, 16, etc.) will also satisfy Eq. (5), so the smallest P value satisfying the rule is taken as the periodicity.

In practice, the droplet quantization rule is applied by testing possible periodicity values—integers from one to half the total number of droplets (N/2)—and noting the P values where the summation expression is exact (in simulations) or where the error in the summation is minimized (in experiments) and reasonably close to zero as shown in Eq. (6). The reason that the maximum observable periodicity value is half the total number of droplets is because in order

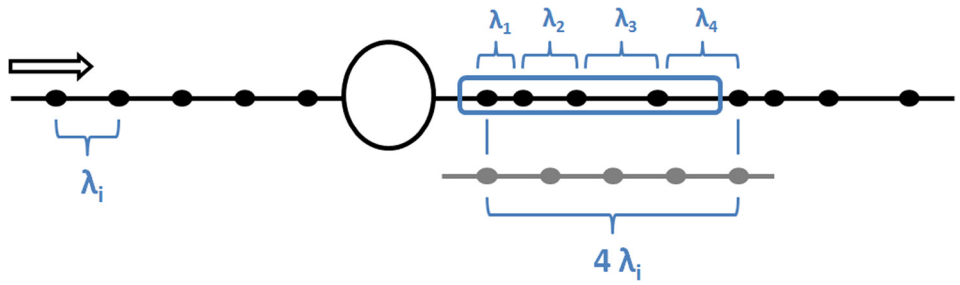

FIG. 4. Illustration of how the droplet spacing quantization method is applied to obtain the periodicity for periodic behaviors.

to safely deem any sequence as periodic, the train must be long enough to see that sequence repeats at least once. If a particular P value satisfies the summation expression no matter which droplet is chosen as the reference point, then that P value is the periodicity—the length of the repeating pattern

$$error = \left| P\lambda_i - \sum_{j=n}^{n+P} \lambda_j \right|. \tag{6}$$

Using the above equation for individual error, the standard deviation from the expected droplet positions, for a given P value, can be calculated by

$$\sigma = \sqrt{\frac{\sum_{n=1}^{N/2} \left(\left| P\lambda_i - \sum_{j=n}^{n+P} \lambda_j \right| \right)^2}{N/2}}. \tag{7}$$

Fig. 5 is the normalized standard deviation of error versus the periodicity values tested for a repeating period-5 pattern observed experimentally. The plot was obtained by testing P values—all integers from one to half of the total number of droplets. For each P value, a series of error values was obtained using Eq. (6) and by varying the reference point (i) from the first exit droplet (closest to the loop exit) to the half-way point in the exit train. The standard deviation in the series was calculated using Eq. (7) and then normalized by the mean input spacing. In Fig. 5, a minimum standard deviation of 0.161 was seen for P = 10, but a very similar standard deviation of 0.163 was seen for P = 5, so the exit pattern exhibited period-5 behavior. After

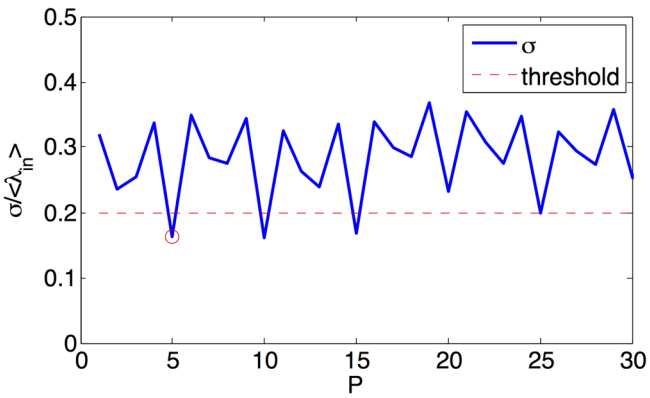

FIG. 5. Plot of standard deviation vs. periodicity values from an experiment exhibiting period-5 behavior, where the standard deviation from the predicted value is normalized by the mean input spacing; dotted red line is an empirically selected threshold below which signifies periodic behavior.

applying the quantization rule to many sets of experimental data, we found that a normalized standard deviation of 0.20 is a suitable maximum threshold for determining whether exit droplet spacings are periodic. This criterion was used in characterizing the exit drop spacing in experiments.

c. Comparison of the two methods. In cases where the bifurcated loop transforms a droplet train of consistent spacing into one with a simple periodic pattern of spacing, both of the previously described characterization methods—Poincare maps and the spacing quantization method—were found to yield the same results. In some specific cases, however, one characterization method is more effective than the other, as described below.

When the exit behavior is intermittent, such as between period-3 and period-4 patterns as shown in Fig. 3(d), the spacing quantization method may yield seemingly aperiodic results when, in fact, there are distinct but separate stretches in time of periodic behavior. This is because the spacing quantization rule in Eq. (5) is designed to work for droplet trains with a single periodic pattern, and the method can only report a single value for the periodicity. Intermittent behaviors are therefore best quantified using animated Poincare maps in which cluster points are highlighted in the order of appearance. Animation allows the viewer to identify separate periodic sequences of map points (see Movies S4, S5, and S6 in the supplementary material).[39]

In some cases, it is possible for one or more clusters of points in a Poincare map to be populated more than once within a periodic pattern, although typically each cluster is populated with only one point per pattern iteration. Figure 6 is an example exit Poincare map for an experiment with an inlet droplet spacing of 19 mm in which the clusters are unequally populated.

Note how the Poincare map suggests that the outlet spacings follow 4-period behavior, as there are 4 clusters. Upon closer inspection, however, we noticed in following each Poincare

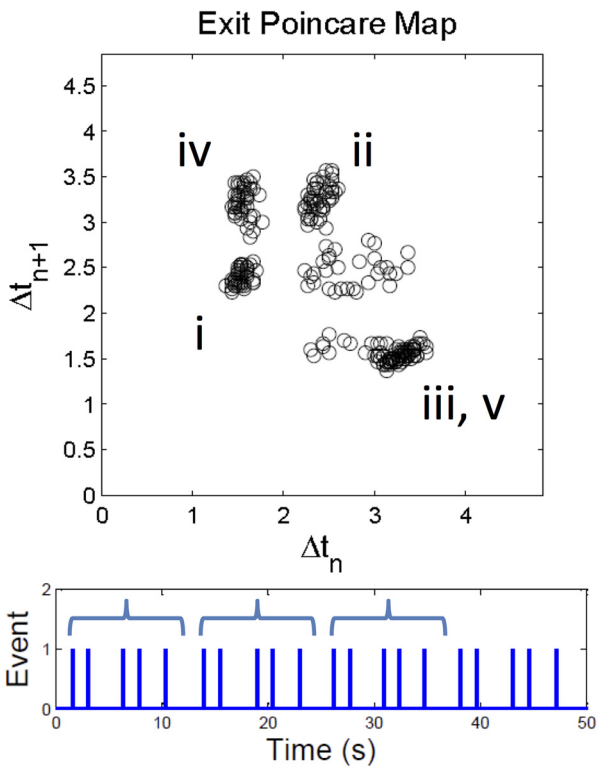

FIG. 6. Exit Poincare map for experimental results for an initial spacing of 19.0 mm and volumetric flow rates (ml/h) of 10, 20, and 2 for main oil, auxiliary oil, and water through a millifluidic bifurcated loop with dimensions as previously described. The numerals represent the order of occurrence of points for the repeating 5-droplet pattern. Beneath the Poincare map is an event-time plot for droplet exit events, with the repeating pattern bracketed.

map point as it was generated that the pattern length was actually five points long, not four. One cluster of points had twice as many occurrences as the other three clusters, which is evident by the numerals showing the order of appearance of each point in the repeating pattern. This 5-droplet pattern could also be seen in the event-time plot in Fig. 6, in which there is clearly a repeating pattern every five events. Thus, in some instances such as this one, Poincare maps can be misleading in characterizing the periodicity. While animation of Poincare maps can be used to identify these scenarios, such animations would need to be reviewed by the user. In contrast, the spacing quantization method can be automated and would immediately return the proper periodicity in cases such as this one, where there is a single, consistent periodic pattern.

3. Comparison of bifurcated loop experiments with model predictions

Using our droplet spacing quantization rule to quantify the periodic behavior in both simulations and experiments and using Poincare maps to quantify intermittent behavior in experiments, we plotted periodicity versus inlet droplet spacing in Figure 7. To assess if we could predict the experimental data in Fig. 7, we performed simulations using the simple network model.[15,31,32] In this model, droplets are treated as point objects, and droplet velocities (U_d) vary proportionally with the mean fluid velocity ($\langle U_f \rangle$): $U_d = \beta \langle U_f \rangle$, where β is an empirically determined slip factor on the order of 1. Each droplet is assumed to increase the resistance in the channel by a fixed amount, R_d. Flow rates in the loop branches depend on the total resistance at any given instant, and they are determined using the relation $\Delta P = Q\ R$, which states that pressure drop is the product of volumetric flow rate and hydrodynamic resistance. When droplets reach the loop entrance, each droplet is placed into whichever branch has the greater flow rate, which is also the path of least resistance. Each time a droplet enters or exits the loop, the total resistances in each branch are recalculated, and the flow rates are updated.

Note, however, that the determination of droplet choice by greatest flow rate is not necessarily valid for other geometries, such as when the cross-sectional areas of branches at the bifurcation are not equal or when there are more than two possible paths. For example, although a specially shaped bifurcated loop has equal flow rates through each branch, an entering droplet always chooses the branch with the narrower cross-sectional area at the entrance.[44] In yet another example, droplets at a 3-way junction choose the path closest to the resultant velocity—sum of all path velocity vectors at the intersection—which is not necessarily the path with the greatest flow rate.[45] A better alternative for describing the path selection is that droplets choose the path based on the net forces at the bifurcation.

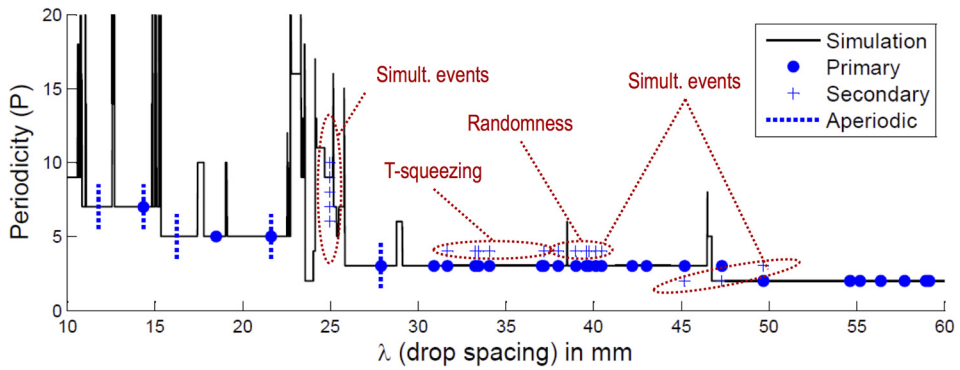

FIG. 7. Comparison of experimental (•, +, - - -) and simulation (—) results on a plot of exit spacing periodicity versus inlet droplet spacing for trains of droplets passing through a millifluidic loop. The simulation results were obtained using an algorithm based on the simple network model to simulate trains of droplets through a bifurcated loop. The spacing quantization method was used to quantify periodic behavior in exit droplet spacing, and Poincare maps were used to quantify intermittent behaviors. Secondary periodic behaviors circled in red were due to simultaneous events, T-squeezing, and/or random decisions due to nearly equal instantaneous branch resistances. Simulation parameters: $Q = 32$ ml/h; $R_d = 3.2 \times 10^{-3}$ kg/mm^4/s; $\beta = 1.2$; I.D. $= 1.25$ mm; $L_u = 44$ mm; are $L_l = 39$ mm.

The drop traffic model has two parameters: R_d and β. To empirically obtain estimates of these parameters, we conducted independent experiments (described in Sec. IV) and measured pressure drop across a linear train of droplets, as well as the individual droplet velocity. We found that $R_d \approx 2-4 \times 10^{-3}$ kg/mm^4/s and $\beta \approx 1.03$–1.12, over a capillary number range (Ca ≈ 0.002–0.009) corresponding to the droplet traffic experiments. We varied R_d and β in this range to obtain a match as close as possible to experimental data. As shown in Fig. 7, we find a good agreement between experiments and simulations, with nearly all of the experimentally observed primary periodic behaviors matching the simulation predictions. To our knowledge, Fig. 7 is the first direct comparison between experiments and simulations of exit dynamics of drops across a wide range of inlet drop spacing.

In many of the experiments, we observed that the exit spacing patterns were not purely one periodic behavior; they instead showed intermittency between two or more periodic and/or aperiodic behaviors. In most of those intermittent cases, a primary periodic behavior was observed, with secondary behaviors occurring less often than the primary behaviors. In Fig. 7, some data points correspond to both primary periodic behavior as well as aperiodic–note how both a solid circle and a dashed vertical bar appear at the same place for those points. In such cases, the behavior was generally periodic, but at certain times throughout the experiment, aperiodic behavior was seen.

We discuss the different sources of intermittent behavior in Sec. II B 4. As is evident in Fig. 7, secondary periodic behaviors typically occur in the vicinity of shifts in primary periodic behavior. For example, the simulations predict a shift from period-3 to period-2 when input spacing increases to about 47 mm. Similarly, the experimental results show the primary periodicity shifting from period-3 to period-2 somewhere between 45 and 50 mm, with both period-2 and period-3 behaviors appearing in the vicinity of the shift.

The degree to which secondary behaviors are seen around shifts in primary periodic behaviors appears to depend on the amount of variation in input spacing. Our syringe pump-driven flows produced input droplet spacings with an average percent relative standard deviation (%RSD) of about 4%–5%. Thus, if the predicted transition from period-3 to period-2 occurs at $\lambda = 47$ mm, we should be able to see both behaviors at least within the range of $\lambda = 47$ mm $\pm$ 5%, or from 44.65 mm to 49.35 mm. In our experiments—as shown in Figure 7—we did in fact see both period-2 and period-3 behaviors in the range of 45 mm to 50 mm. We also tried a few experiments in which we produced droplets using constant pressure (delivered by a Fluigent^{TM} MFCS-FLEX^{TM} pressure-control unit), which enabled us to produce droplet trains with less than 1.0%RSD in inter-droplet spacing. In those initial experiments using the pressure-driven system, we noticed that the span of input spacings where we could see both period-3 and period-2 behaviors shrank to within 1.0 mm, which corresponds to roughly $\pm$1% of the transition point. The degree of input spacing variation therefore appears to directly affect the span of the intermittency region around a behavioral shift.

According to our simulations, if the inlet spacings were all perfectly equal, the exit spacings would always be periodic if a long enough train of droplets was observed. In experiments, however, the unsteadiness of flow always causes fluctuations in incoming droplet spacings. As can be seen in Figure 7, the span of major periodic behaviors generally decreases as inlet spacing decreases. This means that spacing transformations become more sensitive to fluctuations in inlet spacing as inlet spacing decreases. Thus, for relatively small incoming droplet spacings such as in regime (c) of Fig. 3, the apparent aperiodicity in experiments is likely due to fluctuations in inlet spacing.

4. Sources of intermittency and aperiodic behavior

Cybulski and Garstecki[27] reported that multiple stable periodic behaviors within the same experiment are accessible using active control (pressure perturbations/spikes). Maddala *et al.*[24] used traffic simulations to show that intermittent behavior can occur when droplets enter and leave the loop simultaneously. After closely studying many hours of bifurcated loop experiment videos, we discovered three major sources of intermittency that will be described below in

more detail: (1) simultaneous entering and exiting events, (2) channel defects, and (3) nearly equal hydrodynamic resistances in both loop branches.

a. Simultaneous entering and exiting events. Figure 8 shows snapshots where two different period-5 behaviors were observed during a 20-min experiment with constant average inlet spacing (see also Movie S1 in the supplementary material).[39] Each row contains two snapshots before and after the third droplet in the repeating pattern enters the bifurcated loop. In the first case (Fig. 8(a)), the droplet decisions at the loop entrance followed a repeating pattern of down-down-up-down-up [ddudu]. In the second case (Fig. 8(b)), the loop entrance decisions followed a repeating pattern of down-down-down-up-up [ddduu]. In both cases, the first two droplets encountered basically the same scenarios when they reached the loop entrance, so they made the same decisions. The third droplet, despite seeing nearly the same scenario at the loop entrance (compare Figs. 8(a-i) and 8(b-i)), significantly affected the outcome. The different outcomes are reflected in the significantly different Poincare maps (Figs. 8(a-iii) and 8(b-iii); see also Movie S4 in the supplementary material).[39] As we discuss below, the cause for such intermittent behavior is the simultaneous entry and exit of a droplet.

In Fig. 8(a-i), when the third droplet is at the loop entrance, there are three droplets in the lower branch. Note that the group of three in the lower branch includes the droplet that is about to exit. Three drops in the shorter lower branch are enough to make the total resistance in the lower path greater than the resistance of the longer upper branch with one droplet, thus the entering droplet chooses the upper path in Fig. 8(a-ii). In Fig. 8(b-i), when the third droplet reaches the loop entrance, the exiting droplet—while less than a droplet length further downstream than in Fig. 8(a-i)—has just exited the loop, leaving only two droplets in the lower path. With only two droplets in the shorter lower branch, the total resistance of the lower path is still less than that of the upper path, so the droplet at the entrance chooses the lower path in Fig. 8(b-ii). Because we had standard deviations of about 5% in inlet droplet spacing, which could account for the difference in position of the exiting droplet in the two cases, the intermittent behavior here was most likely induced by natural fluctuations in inlet spacing.

This case study suggests that intermittent and aperiodic behaviors occur when entering and exiting events occur simultaneously, and different behaviors are induced by slight fluctuations in inlet spacing. We hypothesize that the larger the inlet fluctuations are, the larger the window of inlet spacings will be that yields intermittent behavior. As a corollary, when there is a generous amount of time between entering and exiting events during periodic behavior, such periodic behavior should be more resilient to fluctuations in inlet spacing.

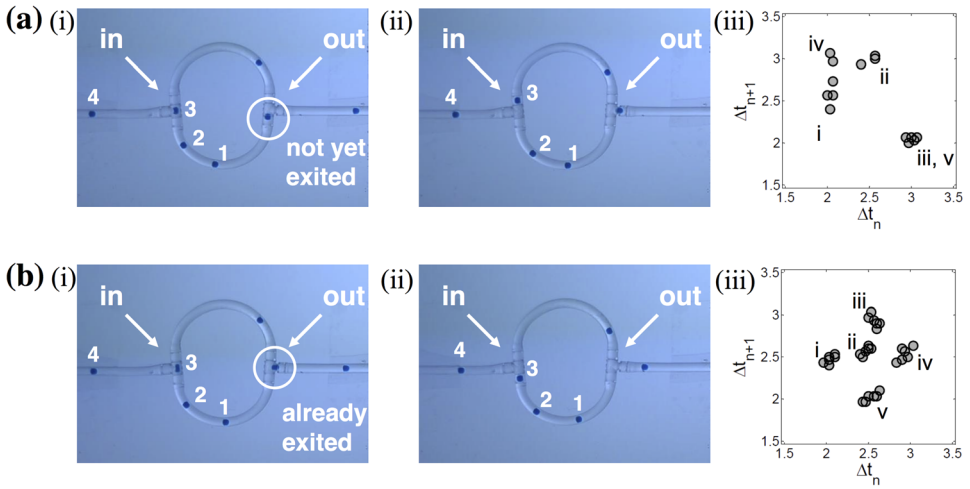

FIG. 8. Snapshots from the same experiment showing intermittency between two different period-5 patterns, where (a-i) and (a-ii) are before and after the third droplet in the first repeating pattern chooses the upper branch, and (b-i) and (b-ii) are before and after the third droplet in the second repeating pattern chooses the lower branch. (a-iii) and (b-iii) show the corresponding Poincare maps for the patterns, with the order of appearance of points denoted by the Roman numerals.

b. Channel defects. A second source of intermittency is the temporary change in confinement of droplets due to channel defects. If there is a channel section where the cross-sectional area changes—e.g., expands, contracts, or changes aspect ratio—the effective hydrodynamic resistance of a droplet temporarily changes as the droplet passes through that section.

Figure 9 illustrates two examples of droplet decisions with and without squeezing of droplets as they pass through slightly crushed tips of T-junction fittings (see also Movie S2 in the supplementary material).[39] The plastic T-junction fittings used in that experiment had fragile tips and were accidentally deformed while attaching tubing. These deformations act as narrowing constrictions that increase the Laplace pressure differential across the water/oil interface at the front of any droplet passing through the constriction. This increase in Laplace pressure at the constriction means that a smaller fraction of the driving pressure is available for driving fluid forward within the channel. With a smaller effective driving pressure, the resulting flow rate decreases, and the shear stresses at the channel entrance (pulling on part of the entering droplet) also decrease.

If the change in flow rate due to T-junction squeezing (or "T-squeezing") of droplets is enough to shift the balance of shear forces from one direction to the other, the droplet decisions will change. For example, in Fig. 9(a-i), where there was no T-junction squeezing of droplets at the critical decision time, the entering droplet chose the lower path as shown in Fig. 9(a-ii). In Fig. 9(b-i), however, the droplet in the lower branch was squeezing through the crimped T-junction fitting near the loop outlet when the entering droplet was at the inlet bifurcation. Flow through the lower path was therefore temporarily impeded, reducing the flow rate in the lower path and the shear stress at the entrance of the lower path. There was enough change in shear stresses at the bifurcation to flip the balance of shear forces on the entering droplet, so the entering droplet chose the upper branch rather than the lower branch (see Fig. 9(b-ii)).

The Poincare maps in Figs. 9(a-iii) and 9(b-iii) correspond to the different exit spacing patterns generated with and without the effects of T-squeezing (see also Movie S5 in the supplementary material).[39] For the conditions and flow rates used to generate Figure 9, when the entering droplet's decision was not affected by T-squeezing—shown in (a)—the resulting behavior was period 3, as can be seen by the three clusters in Fig. 9(a-iii). However, when the entering droplet's decision was altered by T-squeezing, the resulting behavior was period 4, which can be seen by the four clusters in Fig. 9(b-iii). Note that while the period-3 and period-4 behaviors were separately shown in Figs. 9(a) and 9(b), both behaviors would have been seen in a Poincare map of the entire experiment. The two behaviors were separated simply to illustrate how channel defects such as crimped T-junction fittings can cause different intermittent behaviors.

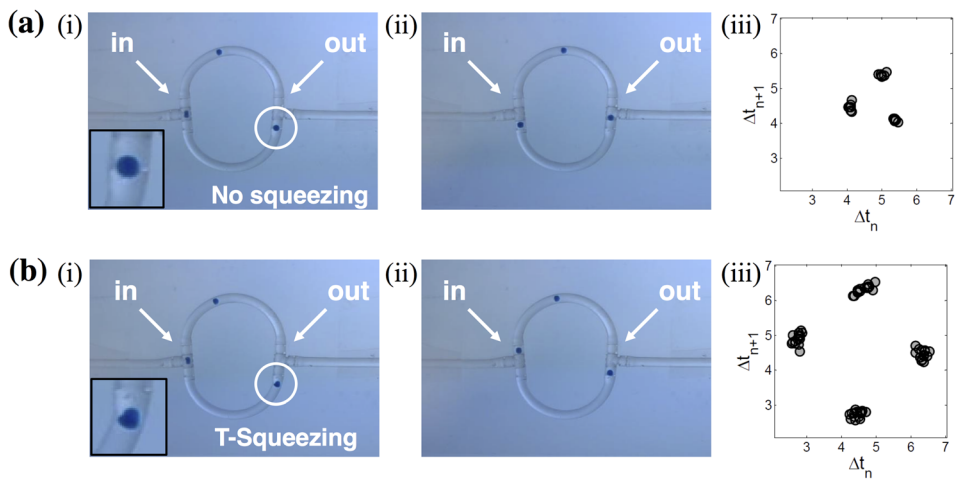

FIG. 9. Intermittent periodic behavior can be caused due to squeezing of droplets at the ends of T-junction adapters. (a) The exiting droplet does not get squeezed (see inset in (i)), and the entering drop chooses the lower branch. This behavior yields a period-3 Poincare map. (b) The exiting droplet undergoes significant squeezing (see inset in (i)), making the entering drop choose the upper branch. This behavior yields a period-4 Poincare map.

c. Nearly equal branch resistances. In some cases, nearly equal resistances in the upper and lower branches result in nearly equal shear stresses at the loop's inlet bifurcation, yielding random droplet decisions. Figure 10 shows two pairs of snapshots taken during the same experiment in which nearly identical conditions yielded opposite results (see also Movie S3 in the supplementary material).[39] Figs. 10(a-i) and 10(b-i) depict virtually identical conditions at different times within the same experiment where there was a droplet at the loop inlet. In both cases, there was one droplet in the upper branch (slightly shorter than the lower), and another droplet just exited the loop. However, in one case, the entering droplet chose the lower branch (Fig. 10(a-ii)), resulting in a period-3 pattern, whereas in the other case, it chose the upper branch (Fig. 10(b-ii)), producing a period-4 pattern (see also Movie S6 in the supplementary material).[39]

The source of these random droplet decisions becomes clear when the droplet resistance is compared with the difference in branch resistances. The difference in length between the longer branch and the shorter branch is 5 mm, which corresponds to a resistance of 2.4×10^{-3} kg/mm^4/s. The droplet resistance is also of a similar value, $R_d \approx 2$ to 3×10^{-3} kg/mm^4/s, for the conditions investigated in this study. Thus, the presence of a single droplet in the shorter branch could almost entirely cancel out the difference in resistance due to the difference in branch lengths. Because the resistances of the upper and lower paths are nearly equal when there is a single droplet in the shorter branch, the up/down decisions of any droplets entering the loop in that state will be uncertain.

C. Investigating droplet traffic in microfluidic versus millifluidic devices

All previous studies have investigated droplet traffic in microfluidic networks, except that of Belloul *et al.*,[29] who investigated droplet behavior at the entrance of a millifluidic bifurcation (and not in a loop, where the branches rejoin). In this study, we investigate drop traffic in a millifluidic loop. Therefore, it is important to delineate the advantages or disadvantages of using microfluidic and millifluidic devices for studying droplet traffic. In this section, we contrast the two approaches with the underlying assumption that microfluidic devices have non-circular cross-section, whereas millifluidic devices are circular in cross-section, although exceptions do exist.[51]

Typical operating parameters for microfluidic and millifluidic experiments are shown in Table I. The volumetric flow rates in microfluidic devices ($Q \approx 0.01$–10 ml/h) are usually lower than those that can be achieved in millifluidic devices ($Q \approx 1$–100 ml/h). Using these estimates of operating flow rates and conduit geometries, we estimate that, in general, the droplet

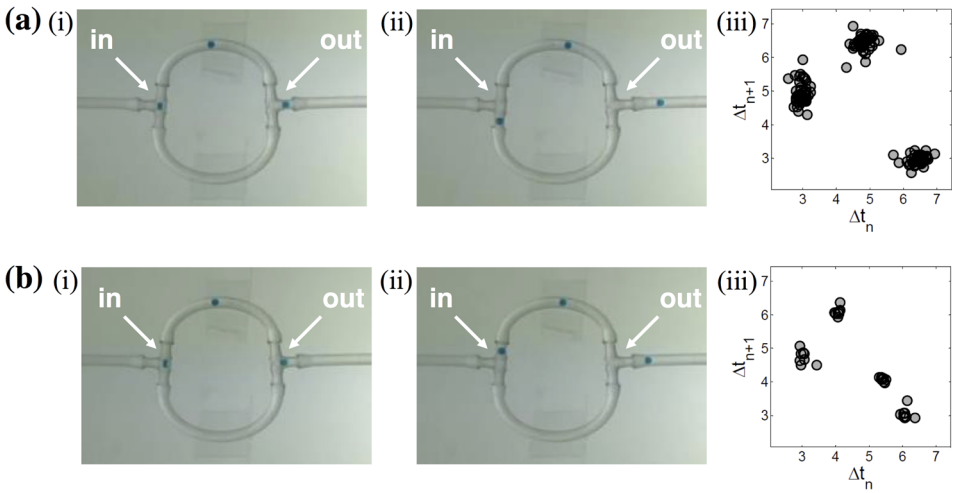

FIG. 10. Example of random droplet decisions when upper and lower path resistances are nearly equal; snapshots before (i) and after (ii) the entering droplet chooses a branch were taken at different times (a) and (b) within the same experiment and show opposite results from virtually identical conditions. Poincare maps (iii) reflect the results of the behaviors shown in (a) and (b).

TABLE I. Order-of-magnitude estimates of flow rates, mean fluid velocities, capillary numbers, droplet frequencies, and observation times in microfluidic and millifluidic devices (e.g., $100 \times 100\,\mu$m microfluidic channels and 1.25 mm I.D. millifluidic channels). The observation times are calculated by dividing the desired number of droplets to be observed ($N = 100$) by the droplet production frequency.

Parameter	Microfluidic	Millifluidic
Flow rate (Q) (ml/h)	0.01–10	1–100
Mean fluid velocity (U) (mm/s)	0.1–100	0.1–10
Capillary number (Ca)	10^{-4}–10^{-1}	10^{-4}–10^{-2}
Drop production frequency (f) (Hz)	10–10^3	0.1–10
Observation time (t_{obs}) (s)	0.1–10	10–10^3

production frequencies range from 10 to 10^3 Hz in microfluidic networks and 0.1–10 Hz in millifluidic networks. Another important parameter is the observation time (t_{obs}) that is directly linked to the number of droplets that need to be recorded for traffic experiments. As shown in Table I, the observation times are much shorter in microfluidic studies compared to millifluidic devices. In Subsections II C 1–II C 5, we consider the consequences of these differences between microfluidic and millifluidic operating parameters.

1. Shear stress for droplet break-up

As discussed in Sec. II B 1, the breakup of droplets at the bifurcation limits the operating regime for drop traffic studies. Since microfluidic channels have gutter flows while circular channels do not, for a fixed flow rate, drops experience larger shear stresses in circular channels than in rectilinear channels. As a result, drops at bifurcations break at lower capillary numbers in millifluidic networks compared to microfluidic networks. This means that the operating regime is smaller for millifluidic compared to microfluidic traffic experiments.

A scaling analysis of the shear stresses (τ) in the rectangular versus circular geometries also supports the two-orders-of-magnitude-smaller values of fitting parameter of Link *et al.* (α_L) found in our millifluidic studies. Since shear stress is proportional to velocity gradient, the shear stress ratio (rectangular-to-circular) is given by

$$\frac{\tau_R}{\tau_C} = \frac{U_R/H}{U_C/h}, \tag{8}$$

where U_R and U_C are the fluid velocity in rectangular and circular channels within the gap, and H and h are the mean fluid gaps in rectangular and circular geometries. Equation (8) can also be expressed as

$$\frac{\tau_R}{\tau_C} = \frac{(Q/\pi DH)/H}{(Q/\pi Dh)/h} = \left(\frac{h}{H}\right)^2. \tag{9}$$

For an idealized cylindrical droplet inscribed within a square channel (note that we assume the square channel has the same hydraulic diameter D as the circular channel), we estimated the mean fluid gap H to be 0.127 D, or about 13% of the diameter. Likewise, the film thickness h in circular channels is 0.7%–3% of the diameter in circular geometry based on the Bretherton[52] relationship, $h/D = 0.669\,Ca^{2/3}$. The shear stress ratio would then be $\tau_R/\tau_C = 0.003$–0.05, which is in reasonable agreement with fitting parameter of Link *et al.* (α_L) of 0.027 found in our millifluidic experiments.

2. Droplet hydrodynamic resistance

The hydrodynamic resistance of droplets is a key parameter in regulating the traffic of droplets in fluidic networks.[53,54] We found that the droplet resistance (R_d) in our millimeter-scale

tubing was at least three orders of magnitude smaller than the droplet resistance observed in rectangular microfluidic channels. Also note that millifluidic networks, which are roughly 10 times as large (in both channel width and length) as their microfluidic counterparts, typically have one to two orders of magnitude smaller pressure drops. In cases where pressures must be maintained below a certain threshold—e.g., to prevent channel walls from deforming—millifluidic networks could accommodate greater numbers of droplets and/or features for the same maximum pressure drop. Millifluidic networks could therefore be more conducive to large-scale drop traffic experiments.

We also estimated the ratio of droplet resistance to the occupied channel resistance (for a channel segment with the same length as the droplet length, l), or R_d/R_c. The ratio R_d/R_c can alternatively be expressed as the length of channel (L_d) with the same resistance as the droplet and normalized by the length of channel (l) occupied by the droplet: L_d/l. Our estimates of L_d/l are presented for our experimental data in comparison with the literature results for short confined droplets in Table II.

Interestingly, we find that although the absolute values of droplet resistance in millifluidic experiments are much smaller than under microfluidic conditions, the normalized droplet resistances are in a similar range (see Table II), indicating that droplet resistance scales with channel resistance. Our empirical observation that droplet resistance is roughly 2–10 times the resistance of the channel segment the droplet occupies[55] could be a useful rule-of-thumb when conducting drop traffic experiments in conduits of different diameter.

3. Duration of video recording of drop traffic

In drop traffic investigations, it is desirable to track a large number of droplets in order to identify periodic and aperiodic behaviors with statistical significance. Because the frequencies of droplet production are 10–10^3 Hz in microfluidic networks and 0.1–10 Hz in millifluidic networks, high-speed cameras are necessary for microfluidics, whereas inexpensive consumer cameras are sufficient for millifluidic applications. In this study, we were able to record 108 000 frames (1 h at 30 fps, 0.03 MB/frame, 3.58 GB) of our millifluidic bifurcated loop experiments using an iPod®, which allowed us to observe 666 droplets. Achieving the same feature at a microfluidic scale would have required high-speed cameras with large RAM (for 108 000 frames at 1 MB/frame using a 1-megapixel high-speed camera, over 100 GB of RAM would be needed), which are prohibitively expensive. Large numbers of droplets can therefore be studied more easily at the millifluidic scale than the microfluidic scale.

4. Role of syringe pump fluctuations

Droplet size and spacing are important parameters regulating drop traffic that are dictated by the flow rates of dispersed and continuous phases.[50] While syringe pumps offer the most convenient means of delivering constant volumetric flow rates in small-scale fluidic devices, they suffer from slight periodic fluctuations.[55] In fact, flow rate fluctuations can be as high as

TABLE II. Comparison of normalized droplet resistances (L_d/l) based on literature data. Bruus's[56] expression for hydrodynamic resistance of rectangular channels and the Hagen-Poiseuille equation were used to calculate the resistance of channels.

Drop length (μm)	Drop aspect ratio (l/w)	Channel dimensions (μm)	R_d (kg/mm^4/s)	L_d/l	Source
400–800 (considering only $l/w < 4$)	2–4	200 × 120	1–3	1.6–2.2	Vanapalli *et al.*[53]
350 (estimated)	1.8	200 × 80	4.5–11	3–7	Bithi and Vanapalli[13]
500–1000 (estimated)	1–2	500 × 300	0.07–0.28	5–10	Labrot *et al.*[46]
1500	1	1500 (circular)	1.2×10^{-3}	2	Sessoms *et al.*[47]
1585 (avg.)	1.25	1270(circular)	$2–4 \times 10^{-3}$	2.7–5.4	This study

10% and recur over time periods ranging from hundreds of Hz to tens of minutes.[55,57–59] Using a time scale analysis of syringe pump fluctuations at the micrometer and millimeter scales, we find that millifluidics—compared to microfluidics—offers a more consistent means of studying droplet traffic when using syringe pumps.

Consider the following two plots of pump flow-rate fluctuations versus time, and note the importance of observation time scale (t_{obs}) relative to pump fluctuation time scale (t_p). In Fig. 11(a), two example observation times of the same duration (t_{obs}^1 and t_{obs}^2) are shown, and both observation times are much shorter than the time period of syringe pump fluctuations (t_p). In contrast, Fig. 11(b) shows an observation time (t_{obs}) much longer than the pump fluctuation time period. As noted by Korczyk *et al.*,[57] while the standard deviation of flow rate in the left scenario (short observation time relative to fluctuation period) might be smaller than that in the right scenario (long observation time relative to fluctuation period), the average flow rate over the observed time will be closer to the actual average when the observation time is large rather than small (relative to the fluctuation period). In scenario (a), two experiments of identical duration and flow rate settings but conducted at different times (t_{obs}^1 and t_{obs}^2) could yield noticeably different average flow rates over the observed times. Such inconsistency is undesirable in studying droplet traffic, where droplet size and spacing are critical to the periodic and/or aperiodic behavior. Scenario (b)—where observation time is much longer than fluctuation period—provides more consistent, predictable results for a given set of flow rates.

To help us to compare the consistency of flow rates in various microfluidic and millifluidic scenarios, we define τ to be the ratio of the syringe pump fluctuation time period (t_p) and the experimental observation time (t_{obs})

$$\tau = \frac{t_p}{t_{obs}} \ . \tag{10}$$

As mentioned above, experimentally observed flow rate behaviors will be more consistent in the case where the observation time (t_{obs}) is much larger than the pump fluctuation period (t_p). This means that small time scale ratios ($\tau \ll 1$) will be better for studying droplet traffic. For large time scale ratios ($\tau \gg 1$), repeated experiments at the same settings could yield different average flow rates and different standard deviations.

Korczyk *et al.* proposed an expression for estimating the time scale of pump fluctuations (t_p) based on flow rate (Q), syringe diameter (D), and pitch of the pump's driving screw (a). Assuming that the same syringe pump is used in comparing microfluidic and millifluidic experiments (constant pitch, a)

$$t_p \propto \frac{D^2}{Q} \ . \tag{11}$$

Next, let us compare time scale ratios between millifluidic and microfluidic cases (τ^m and τ^μ) in several scenarios. Using Eqs. (10) and (11), the following relation can be derived for comparing the millifluidic and microfluidic time scale ratios:

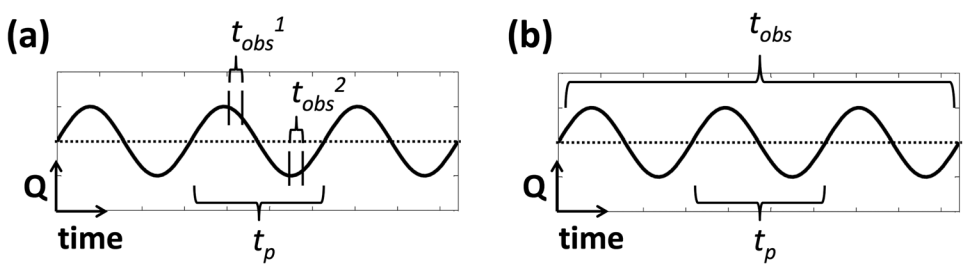

FIG. 11. Comparison of pump fluctuation time scale (t_p) with observation time scale (t_{obs}) on hypothetical plots of volumetric flow rate versus time. (a) $t_{obs} \ll t_p$; and (b) $t_{obs} \gg t_p$.

$$\frac{\tau^m}{\tau^\mu} = \frac{t_p^m / t_{obs}^m}{t_p^\mu / t_{obs}^\mu} = \left(\frac{D^m}{D^\mu}\right)^2 \left(\frac{Q^\mu}{Q^m}\right) \left(\frac{t_{obs}^\mu}{t_{obs}^m}\right). \quad (12)$$

Assuming average observation times of 100 s and 1 s in millifluidic and microfluidic experiments, respectively (see Table I), Table III shows how millifluidic and microfluidic time scale ratios compare in various combinations of syringe sizes and flow rates.

As seen in Table III, $\tau^m/\tau^\mu \leq 1$, so the millifluidic time scale ratio is always less than or equal to the microfluidic time scale ratio. Therefore, in all cases, the millifluidic scale experiments would be as good as or better than microfluidic scale experiments in generating consistent droplet trains when using syringe pumps.

5. Flexibility in designing fluidic networks

To demonstrate the flexibility of millifluidic networks, we also assembled millimeter-scale versions of other microfluidic networks that have been previously studied: a ladder network (Fig. 12(a)) and a parking network (Figs. 12(b) and 12(c)). All of these networks were created by simply joining lengths of commercially available Tygon® tubing and plastic T-fittings. For the parking network in Figs. 12(b) and 12(c), a constriction for trapping droplets was formed by inserting a short section of smaller-diameter Tygon® tubing into the larger-diameter Tygon® tubing.

Fig. 12(a) includes two time lapse snapshots of a millifluidic ladder network showing how such a network can be used to decrease the longitudinal spacing between pairs of droplets. Both the upper and lower sides of the ladder have identical input volumetric flow rates. The interconnecting sections of the network ("bypasses" or "ladder rungs"), however, redistribute flow so that pairs of droplets tend towards synchronizing their longitudinal positions.[60] The behavior we saw in the millifluidic ladder network mimics the synchronizing behaviors seen in microfluidic versions as reported by Prakash and Gershenfeld and Maddala *et al.*[15,60] We initially had very long and separate exit tubes for our millifluidic networks and encountered problems with different numbers of droplets in the two sides of the ladder exit creating unequal resistances. This prevented droplet spacings from being maintained at the exit. In less than 10 min, we were able to solve the problem by reconfiguring the ladder exit with two relatively short side segments joining into a single exit tube (see also Movie S7 in the supplementary material).[39]

Figure 12(b) shows a parking network filled with dye to highlight the two paths available for fluid as it reaches a bifurcation: an upper path (or "bypass") and a lower path, which combine into a single exit (see also Movie S8 in the supplementary material).[39] The lower path has slightly greater resistance than the upper path so that droplets initially choose the upper path. Once there are enough droplets in the upper branch to increase the total resistance of the upper path beyond that of the lower path, the next droplet will choose the lower path. Note that the lower path contains a narrow constriction. This constriction allows the continuous phase fluid to pass but prevents droplets from passing—thereby parking (or "trapping") them, as seen in Fig. 12(c)—so long as the pressure differential across the parked droplet is sufficiently low. Because the individual droplet resistances were unknown, successful trapping required many

TABLE III. Various conditions and the resulting comparison between millifluidic and microfluidic time scale ratios (τ^m/τ^μ). Syringe sizes are compared using their diameters in the milli- and micro-fluidic cases (D^m, D^μ), and the ratios of milli- and micro-scale flow rates are also given (Q^m/Q^μ).

Conditions	D^m/D^μ	Q^m/Q^μ	τ^m/τ^μ
Same syringe, same Q	1	1	10^{-2}
Same syringe, different Q	1	10	10^{-4}
Different syringe, same Q	10	1	1
Different syringe, different Q	10	100	10^{-2}

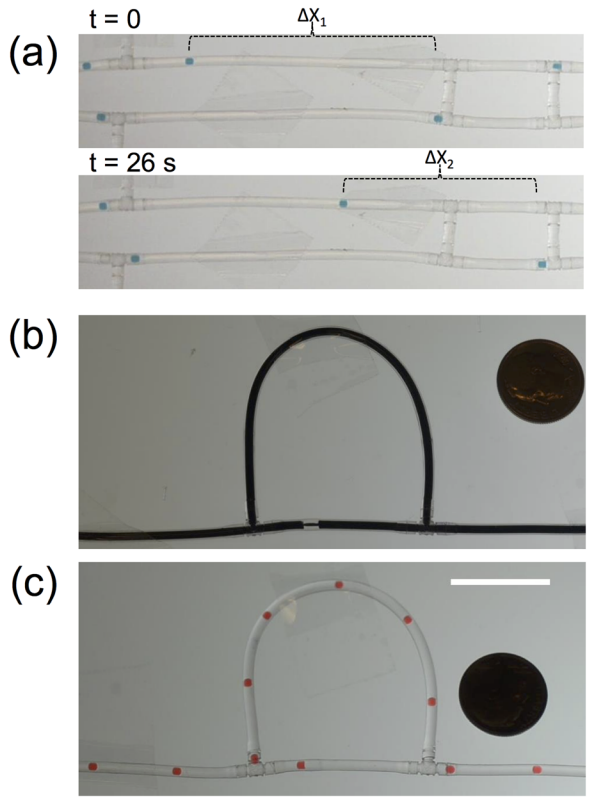

FIG. 12. Example millifluidic ladder and trapping networks. The networks were assembled using commercial T fittings. (a) A ladder network before and after one of two drops in the inlet segments passes the first bypass channel; the longitudinal drop spacing decreases due to bypass flow: $\Delta X_2 < \Delta X_1$; (b) a parking network filled with black dye to illustrate the fluid paths, and (c) the same parking network after trapping one droplet in a train of droplets. Scale bar is 20 mm for (a)–(c).

iterations of changing bypass lengths and trying different constriction diameters and lengths. These changes, however, took relatively little time, as new designs were created by merely disconnecting tubing segments from T-fittings and replacing various segments with different sizes. We were able to successfully park aqueous droplets (in a mineral oil continuous phase) using our millifluidic parking network, which could serve as a useful tool for studying traffic through microfluidic parking networks.[13,61–65]

The relative ease with which modular millifluidic loop, ladder, and parking networks were assembled, combined with the similarity in behavior between the millifluidic and microfluidic counterparts, highlights the usefulness of modular millifluidics as a tool for studying droplet traffic.

III. CONCLUSIONS

We showed that modular millifluidic networks are simpler, more cost-effective alternatives to traditional microfluidic networks, and they can be rapidly generated and altered to optimize designs. Droplet traffic can also be studied more conveniently and inexpensively at the millimeter scale, as droplets are readily visible to the naked eye. Inexpensive consumer electronics such as iPod® media players, smart phones, and digital cameras can be used for imaging and video recording. The ease of visualization of flows in millifluidic devices lends itself not only to scientific research but also to the education of students in science and engineering. Millifluidic devices can be used to introduce concepts such as laminar flow, flow reversibility, deformation of soft objects due to shear stress, and nonlinear dynamics.

To demonstrate the flexibility and potential of modular millifluidics, we created a bifurcated loop network using only Tygon® tubing and plastic T-junction fittings. We quickly

scanned the experimental conditions and identified the parameter space where drop traffic can be investigated. We observed the same types of periodic and aperiodic transformations of evenly spaced input droplet trains as seen in millifluidic bifurcated loops. Our experimental results of primary periodic behaviors as a function of inlet drop spacing were in good agreement with simulations based on the simple network model.

For periodic transformations of input droplet spacings using a millifluidic bifurcated loop, we find that the spacing quantization method is a more reliable means for characterizing periodicity than Poincare maps. The spacing quantization method, however, is not suitable for intermittent behaviors and cannot distinguish between intermittent and aperiodic transformations. Applying the spacing quantization rule in network model-based simulations, we found good agreement between simulation and experimental results.

We found three main sources of intermittency between different periodic and/or aperiodic behaviors in experiments: (1) simultaneous entering and exiting events, (2) channel defects, and (3) equal or nearly equal hydrodynamic resistances in both sides of the bifurcated loop. In cases of simultaneous events and/or channel defects, the range of input spacings where intermittent behaviors will be seen depends on the degree of inherent variation in input spacing. Finally, we contrast important differences between millifluidic and microfluidic experiments and the benefits offered by conducting drop traffic studies at the millimeter-scale.

IV. MATERIALS AND METHODS

A. Drop traffic experiments

We used syringe pumps (Harvard Apparatus, PHD 2000) to deliver constant volumetric flow rates of mineral oil (Sigma Aldrich) and deionized water with 1 wt. % food dye (Great Value, assorted colors), and we produced immiscible aqueous droplets with a T-junction upstream of the desired network. Interfacial tension of 22 mN/m was measured using a Kruss K100 force tensiometer. The slightly asymmetric bifurcated loop had a 39 mm shorter branch and a 44 mm longer branch. All of the millifluidic devices were made from Tygon® microbore tubing, 0.050 in./1.25 mm inner diameter (ID) and 0.090 in. (2.29 mm) outer diameter (OD), and milli-T-junctions (polypropylene tube-to-tube connectors—designed for 1.6 mm ID tubing—from Value Plastics, Inc.). The total flow rates ranged from 10 to 100 ml/h, with droplet production water-to-oil ratios ranging from 0.1 to 0.2 in our final experiments. An optional auxiliary oil flow (using a second T-junction after the first) was also used at times to increase input spacing.

Millifluidic parking networks were also studied in a manner similar to that used for the bifurcated loop. The lower branch had a short segment of smaller-diameter Tygon® tubing (0.5 mm ID) snugly inserted to act as a constriction for trapping drops. Various upper channel (or "bypass") lengths were used to obtain different trapping patterns.

Experimental videos at 30 frames per second were recorded using an iPod® Touch (Apple, 32 GB, 5th generation). A webcam interfaced with Matlab via a custom script was used for real-time monitoring of inlet droplet spacing, and a U.S. dime (17.91 mm diameter) was included in the viewing area for automated pixel-to-length scaling. ImageJ software (NIH) was used to manually verify pixel-to-length scaling.

For the bifurcated loop experiments, custom Matlab scripts were used for post-experiment image analysis to report droplet spacing in the exit channel, generate Poincare maps (including animated Poincare maps that show the order of appearance of map clusters), generate event-time plots of droplet exit events, and apply the droplet spacing quantization rule to characterize the transformation of droplet spacing.

B. Measurement of hydrodynamic resistance of droplets

To properly simulate droplet traffic through millifluidic networks requires realistic values for the hydrodynamic resistance of droplets in millimeter-scale round channels. We obtained an empirical range for droplet resistance ("R_d") in our expected operating conditions by sending a

train of droplets through a 1.54 m length of 1.25 mm ID Tygon® tubing at various constant volumetric flow rates, then measuring the pressure drops across the length ("L_c") of the channel (or tubing) and counting the number of droplets in the tubing after the pressure gauge. A T-junction was used to produce aqueous droplets with 1% w/w food dye in a continuous phase of mineral oil. To vary the droplet velocities—and therefore the capillary number—a second T-junction downstream of the first was used to introduce additional mineral oil. A digital pressure gauge was used to measure the pressure at a point just downstream of the second T-junction.

The Hagen-Poiseuille equation, which governs the laminar flow of incompressible Newtonian fluids, can be recast as an analogue of Ohm's law, where pressure drop ($-\Delta P$) is the product of volumetric flow rate (Q) and the total hydrodynamic resistance.[25,31,32] Assuming that the resistance of each droplet is additive

$$-\Delta P = Q \cdot \left(\frac{8\mu L_c}{\pi r^4} + nR_d \right), \tag{13}$$

where μ is the viscosity of the continuous phase, L_c is the length of the channel (or tubing), r is the radius of the fluid path, and n is the number of droplets in the length L_c. Droplet resistance (R_d) is then

$$R_d = \frac{1}{n} \left(\frac{-\sum P}{Q} - \frac{8\mu L_c}{\pi r^4} \right). \tag{14}$$

We experimentally obtained droplet resistance values ranging from 2×10^{-3} to 4×10^{-3} kg/mm^4/s in the range of Ca numbers seen in our bifurcated loop experiments: $2 \times 10^{-3} \leq Ca \leq 9 \times 10^{-3}$. We also observed the droplet velocity slip factor, β, to increase slightly with increasing Ca number. Slip-factor (β, ratio of droplet velocity to mean continuous phase fluid velocity) ranged from 1.03 to 1.12 and increased gradually with increasing Ca.

ACKNOWLEDGMENTS

This work was supported by the National Science Foundation (CDI-Type 1, #1124814). We benefited from stimulating discussions with Raghunathan Rengaswamy and Jeevan Maddala. We would also like to acknowledge Daphne Tran Huynh, Alex Nunez, and Braden Pate for experimental support.

[1]H. Song, D. L. Chen, and R. F. Ismagilov, "Reactions in droplets in microfluidic channels," Angew. Chem., Int. Ed. **45**, 7336 (2006).
[2]D. T. Chiu, R. M. Lorenz, and G. D. Jeffries, "Droplets for ultrasmall-volume analysis," Anal. Chem. **81**, 5111 (2009).
[3]M. T. Guo, A. Rotem, J. A. Heyman, and D. A. Weitz, "Droplet microfluidics for high-throughput biological assays," Lab Chip **12**, 2146 (2012).
[4]D. G. Anderson, S. Levenberg, and R. Langer, "Nanoliter-scale synthesis of arrayed biomaterials and application to human embryonic stem cells," Nat. Biotechnol. **22**, 863 (2004).
[5]K. M. Schultz and E. M. Furst, "High-throughput rheology in a microfluidic device," Lab Chip **11**, 3802 (2011).
[6]R. K. Shah *et al.*, "Designer emulsions using microfluidics," Mater. Today **11**, 18 (2008).
[7]D. Dendukuri, K. Tsoi, T. A. Hatton, and P. S. Doyle, "Controlled synthesis of nonspherical microparticles using microfluidics," Langmuir **21**, 2113 (2005).
[8]A. W. Martinez, S. T. Phillips, E. Carrilho, S. W. Thomas III, H. Sindi, and G. M. Whitesides, "Simple telemedicine for developing regions: Camera phones and paper-based microfluidic devices for real-time, off-site diagnosis," Anal. Chem. **80**, 3699 (2008).
[9]W. G. Lee, Y.-G. Kim, B. G. Chung, U. Demirci, and A. Khademhosseini, "Nano/microfluidics for diagnosis of infectious diseases in developing countries," Adv. Drug Delivery Rev. **62**, 449 (2010).
[10]G. F. Christopher and S. L. Anna, "Microfluidic methods for generating continuous droplet streams," J. Phys. D: Appl. Phys. **40**, R319 (2007).
[11]G. M. Whitesides, "The origins and the future of microfluidics," Nature **442**, 368 (2006).
[12]G. Cristobal, J.-P. Benoit, M. Joanicot, and A. Ajdari, "Microfluidic bypass for efficient passive regulation of droplet traffic at a junction," Appl. Phys. Lett. **89**, 034104 (2006).
[13]S. S. Bithi and S. A. Vanapalli, "Behavior of a train of droplets in a fluidic network with hydrodynamic traps," Biomicrofluidics **4**, 044110 (2010).

[14]P. Abbyad, R. Dangla, A. Alexandrou, and C. N. Baroud, "Rails and anchors: Guiding and trapping droplet microreactors in two dimensions," Lab Chip **11**, 813 (2011).
[15]M. Prakash and N. Gershenfeld, "Microfluidic bubble logic," Science **315**, 832 (2007).
[16]J. Hong, M. Choi, J. B. Edel, and A. J. deMello, "Passive self-synchronized two-droplet generation," Lab Chip **10**, 2702 (2010).
[17]B. Ahn, K. Lee, H. Lee, R. Panchapakesan, and K. W. Oh, "Parallel synchronization of two trains of droplets using a railroad-like channel network," Lab Chip **11**, 3956 (2011).
[18]L. Ménétrier-Deremble and P. Tabeling, "Droplet breakup in microfluidic junctions of arbitrary angles," Phys. Rev. E **74**, 035303 (2006).
[19]S. Protiere, M. Bazant, D. Weitz, and H. Stone, "Droplet breakup in flow past an obstacle: A capillary instability due to permeability variations," Europhys. Lett. **92**, 54002 (2010).
[20]L. Salkin, L. Courbin, and P. Panizza, "Microfluidic breakups of confined droplets against a linear obstacle: The importance of the viscosity contrast," Phys. Rev. E **86**, 036317 (2012).
[21]W. Engl, M. Roche, A. Colin, P. Panizza, and A. Ajdari, "Droplet traffic at a simple junction at low capillary numbers," Phys. Rev. Lett. **95**, 208304 (2005).
[22]T. Glawdel, C. Elbuken, and C. Ren, "Passive droplet trafficking at microfluidic junctions under geometric and flow asymmetries," Lab Chip **11**, 3774 (2011).
[23]J. Maddala, B. Srinivasan, S. S. Bithi, S. A. Vanapalli, and R. Rengaswamy, "Design of a model-based feedback controller for active sorting and synchronization of droplets in a microfluidic loop," AIChE J. **58**, 2120 (2012).
[24]J. Maddala, S. A. Vanapalli, and R. Rengaswamy, "Origin of periodic and chaotic dynamics due to drops moving in a microfluidic loop device," Phys. Rev. E **89**, 023015 (2014).
[25]F. Jousse, R. Farr, D. R. Link, M. J. Fuerstman, and P. Garstecki, "Bifurcation of droplet flows within capillaries," Phys. Rev. E **74**, 036311 (2006).
[26]M. J. Fuerstman, P. Garstecki, and G. M. Whitesides, "Coding/decoding and reversibility of droplet trains in microfluidic networks," Science **315**, 828 (2007).
[27]O. Cybulski and P. Garstecki, "Dynamic memory in a microfluidic system of droplets traveling through a simple network of microchannels," Lab Chip **10**, 484 (2010).
[28]D. Sessoms, A. Amon, L. Courbin, and P. Panizza, "Complex dynamics of droplet traffic in a bifurcating microfluidic channel: Periodicity, multistability, and selection rules," Phys. Rev. Lett. **105**, 154501 (2010).
[29]M. Belloul, W. Engl, A. Colin, P. Panizza, and A. Ajdari, "Competition between local collisions and collective hydrodynamic feedback controls traffic flows in microfluidic networks," Phys. Rev. Lett. **102**, 194502 (2009).
[30]M. Belloul, L. Courbin, and P. Panizza, "Droplet traffic regulated by collisions in microfluidic networks," Soft Matter **7**, 9453 (2011).
[31]M. Schindler and A. Ajdari, "Droplet traffic in microfluidic networks: A simple model for understanding and designing," Phys. Rev. Lett. **100**, 044501 (2008).
[32]F. Jousse, G. P. Lian, R. Janes, and J. Melrose, "Compact model for multi-phase liquid-liquid flows in micro-fluidic devices," Lab Chip **5**, 646 (2005).
[33]J. Maddala and R. Rengaswamy, "Design of multi-functional microfluidic ladder networks to passively control droplet spacing using genetic algorithms," Comput. Chem. Eng. **60**, 413 (2014).
[34]V. Trivedi, A. Doshi, G. Kurup, E. Ereifej, P. Vandevord, and A. S. Basu, "A modular approach for the generation, storage, mixing, and detection of droplet libraries for high throughput screening," Lab Chip **10**, 2433 (2010).
[35]L. Baraban, F. Bertholle, M. L. Salverda, N. Bremond, P. Panizza, J. Baudry, J. A. G. de Visser, and J. Bibette, "Millifluidic droplet analyser for microbiology," Lab Chip **11**, 4057 (2011).
[36]T. Bowman, J. Frechette, and G. Drazer, "Force driven separation of drops by deterministic lateral displacement," Lab Chip **12**, 2903 (2012).
[37]N. Lorber *et al*., "Some recent advances in the design and the use of miniaturized droplet-based continuous process: Applications in chemistry and high-pressure microflows," Lab Chip **11**, 779 (2011).
[38]P. Panizza, W. Engl, C. Hany, and R. Backov, "Controlled production of hierarchically organized large emulsions and particles using assemblies on line of co-axial flow devices," Colloids Surf., A **312**, 24 (2008).
[39]See supplementary material at http://dx.doi.org/10.1063/1.4902910 for experiment videos of intermittency from a millifluidic bifurcated loop, associated animated Poincare maps, and other example millifluidic networks.
[40]A. Amon, A. Schmit, L. Salkin, L. Courbin, and P. Panizza, "Path selection rules for droplet trains in single-lane microfluidic networks," Phys. Rev. E **88**, 013012 (2013).
[41]M. D. Behzad, H. Seyed-Allaei, and M. R. Ejtehadi, "Simulation of droplet trains in microfluidic networks," Phys. Rev. E **82**, 037303 (2010).
[42]R. Jeanneret, J.-P. Vest, and D. Bartolo, "Hamiltonian traffic dynamics in microfluidic-loop networks," Phys. Rev. Lett. **108**, 034501 (2012).
[43]P. Parthiban and S. A. Khan, "Filtering microfluidic bubble trains at a symmetric junction," Lab Chip **12**, 582 (2012).
[44]W. Choi, M. Hashimoto, A. K. Ellerbee, X. Chen, K. J. Bishop, P. Garstecki, H. A. Stone, and G. M. Whitesides, "Bubbles navigating through networks of microchannels," Lab Chip **11**, 3970 (2011).
[45]J. Y. Moon, S. Kondaraju, W. Choi, and J. S. Lee, "Lattice Boltzmann-immersed boundary approach for vesicle navigation in microfluidic channel networks," Microfluid. Nanofluid. (published online 2014).
[46]V. Labrot, M. Schindler, P. Guillot, A. Colin, and M. Joanicot, "Extracting the hydrodynamic resistance of droplets from their behavior in microchannel networks," Biomicrofluidics **3**, 012804 (2009).
[47]D. A. Sessoms, M. Belloul, W. Engl, M. Roche, L. Courbin, and P. Panizza, "Droplet motion in microfluidic networks: Hydrodynamic interactions and pressure-drop measurements," Phys. Rev. E **80**, 016317 (2009).
[48]B. J. Smith and D. P. Gaver III, "Agent-based simulations of complex droplet pattern formation in a two-branch microfluidic network," Lab Chip **10**, 303 (2010).
[49]D. Link, S. L. Anna, D. Weitz, and H. Stone, "Geometrically mediated breakup of drops in microfluidic devices," Phys. Rev. Lett. **92**, 054503 (2004).

[50]P. Garstecki, M. J. Fuerstman, H. A. Stone, and G. M. Whitesides, "Formation of droplets and bubbles in a microfluidic T-junction—scaling and mechanism of break-up," Lab Chip **6**, 437 (2006).
[51]L. K. Fiddes, N. Raz, S. Srigunapalan, E. Tumarkan, C. A. Simmons, A. R. Wheeler, and E. Kumacheva, "A circular cross-section PDMS microfluidics system for replication of cardiovascular flow conditions," Biomaterials **31**, 3459 (2010).
[52]F. Bretherton, "The motion of long bubbles in tubes," J. Fluid Mech. **10**, 166 (1961).
[53]S. A. Vanapalli, A. G. Banpurkar, D. van den Ende, M. H. Duits, and F. Mugele, "Hydrodynamic resistance of single confined moving drops in rectangular microchannels," Lab Chip **9**, 982 (2009).
[54]B. J. Adzima and S. S. Velankar, "Pressure drops for droplet flows in microfluidic channels," J. Micromech. Microeng. **16**, 1504 (2006).
[55]T. Glawdel and C. L. Ren, "Global network design for robust operation of microfluidic droplet generators with pressure-driven flow," Microfluid. Nanofluid. **13**, 469 (2012).
[56]H. Bruus, *Theoretical Microfluidics* (Oxford University Press, 2008), Vol. 18.
[57]P. M. Korczyk, O. Cybulski, S. Makulska, and P. Garstecki, "Effects of unsteadiness of the rates of flow on the dynamics of formation of droplets in microfluidic systems," Lab Chip **11**, 173 (2011).
[58]Z. Li, S. Y. Mak, A. Sauret, and H. C. Shum, "Syringe-pump-induced fluctuation in all-aqueous microfluidic system implications for flow rate accuracy," Lab Chip **14**, 744 (2014).
[59]N. de Mas, A. Günther, T. Kraus, M. A. Schmidt, and K. F. Jensen, "Scaled-out multilayer gas-liquid microreactor with integrated velocimetry sensors," Ind. Eng. Chem. Res. **44**, 8997 (2005).
[60]J. Maddala, W. S. Wang, S. A. Vanapalli, and R. Rengaswamy, "Traffic of pairs of drops in microfluidic ladder networks with fore-aft structural asymmetry," Microfluid. Nanofluid. **14**, 337 (2013).
[61]M. Sun, S. S. Bithi, and S. A. Vanapalli, "Microfluidic static droplet arrays with tuneable gradients in material composition," Lab Chip **11**, 3949 (2011).
[62]C. H. Schmitz, A. C. Rowat, S. Köster, and D. A. Weitz, "Dropspots: A picoliter array in a microfluidic device," Lab Chip **9**, 44 (2009).
[63]A. Huebner, D. Bratton, G. Whyte, M. Yang, A. J. deMello, C. Abell, and F. Hollfelder, "Static microdroplet arrays: A microfluidic device for droplet trapping, incubation and release for enzymatic and cell-based assays," Lab Chip **9**, 692 (2009).
[64]H. Boukellal, Š. Selimović, Y. Jia, G. Cristobal, and S. Fraden, "Simple, robust storage of drops and fluids in a microfluidic device," Lab Chip **9**, 331 (2009).
[65]S. S. Bithi, W. S. Wang, M. Sun, J. Blawzdziewicz, and S. A. Vanapalli, "Coalescing drops in microfluidic parking networks: A multifunctional platform for drop-based microfluidics," Biomicrofluidics **8**, 034118 (2014).